Mitigating the Water Sensitivity of PBAT/TPS Blends through the Incorporation of Lignin-Containing Cellulose Nanofibrils for Application in Biodegradable Films

Mohamed Aouay, Albert Magnin, Christine Lancelon-Pin, Jean-Luc Putaux, Sami Boufi

ACS Sustainable Chemistry & Engineering

pubs.acs.org/journal/ascecg

Research Article

Mitigating the Water Sensitivity of PBAT/TPS Blends through the Incorporation of Lignin-Containing Cellulose Nanofibrils for Application in Biodegradable Films

Mohamed Aouay, Albert Magnin, Christine Lancelon-Pin, Jean-Luc Putaux, and Sami Boufi*

Cite This: ACS Sustainable Chem. Eng. 2024, 12, 10805−10819

Read Online

ACCESS | Metrics & More | Article Recommendations | Supporting Information

ABSTRACT: Poly(butylene adipate terephthalate)/thermoplastic starch (PBAT/TPS) blends are a significant family of biodegradable plastics holding more than 10% of the market share with widespread applications such as biodegradable bags and mulching films. However, in commercial PBAT/TPS blends, the TPS content seldom exceeds 20−30 wt % since the TPS phase negatively impacts the mechanical properties of the film and increases the water sensitivity. This increases the cost of the material and reduces its biobased content. To address this limitation, up to 10 wt % lignin-containing cellulose nanofibrils (LCNFs) with a significant lignin content (around 20 wt %) were added to PBAT/TPS blends using twin-screw extrusion. The mechanical, morphological, rheological, and water sorption properties of the films were then investigated. The incorporation of LCNFs positively influenced both the ultimate strength and tensile modulus, without sacrificing ductility. Scanning electron microscopy images revealed a nodular morphology of TPS, and the inclusion of LCNFs induced an increase in the size of the dispersed TPS nodules, accompanied by a broadening of the size distribution. The addition of LCNFs also resulted in an increase in the melt stiffness of the blend and a substantial reduction in moisture sorption at both normal and high relative humidity levels, markedly contributing to mitigating the water sensitivity of PBAT/TPS blends. As a proof of concept, thin films from PBAT/TPS/LCNF blends were fabricated through blown-film extrusion, confirming that the incorporation of LCNFs did not impact the material processing. The results offer a sustainable, fully biobased alternative to improve the mechanical properties, mitigate water sensitivity in PBAT/TPS blends, and concomitantly increase their biobased content.

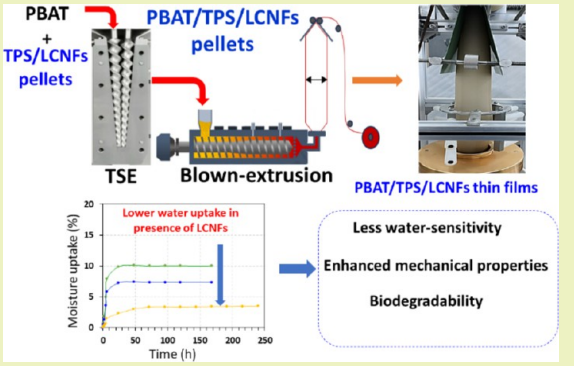

KEYWORDS: *lignin-containing cellulose nanofibrils, poly(butylene adipate terephthalate), thermoplastic starch, composites, biodegradation*

1. INTRODUCTION

Lignin-containing cellulose nanofibrils (LCNFs) have recently received great interest as a new class of nanoscale lignocellulosic material, driven by the additional functionalities brought (induced) by the presence of lignin in LCNFs. In contrast to conventional CNFs, exempt of lignin, LCNFs demonstrate a hydrophobic character, higher thermostability, UV absorption, lower water sensitivity, self-bonding over a critical temperature, and even improved barrier properties, among others.[1,2] Another significant advantage of LCNFs lies in their ability to enhance the sustainability and circularity of biomass processing, requiring fewer chemicals compared to the preparation of CNFs. Unlike the conventional CNF production process, which involves fully removing lignin from cellulose fibers through soda cooking or the kraft process, followed by a bleaching treatment, LCNFs reduce the consumption of chemicals and minimize effluent generation, simplifying the overall treatment process.

In nanocomposite materials, the presence of lignin in LCNFs contributes to enhancing the dispersion of CNF nanofillers within the polymer matrix. This improvement is attributed to the hydrophobic characteristics of lignin, which mitigates the inherent tendency of CNFs to strongly and irreversibly aggregate upon the removal of water by evaporation. The literature has extensively discussed the superior dispersion of LCNFs in hydrophobic polymer matrices and their enhanced compatibility with the polymer matrix.[3−6] For instance, in poly(lactic acid)-based composites, the inclusion of lignin enhanced interfacial interactions and

Received: March 15, 2024
Revised: June 19, 2024
Accepted: June 21, 2024
Published: July 8, 2024

compatibility between LCNFs and the PLA matrix. This resulted in significantly improved mechanical properties of PLA/LCNF composite films, coupled with excellent UV-shielding, water vapor barrier properties, and strong thermal stability.[7]

The lower susceptibility of LCNFs to water has garnered interest in their combination with thermoplastic starch (TPS) matrices to enhance the mechanical properties and reduce the water sensitivity of TPS. In this regard, Zhang et al. prepared LCNFs by mechanically fibrillating unbleached tree bark after alkaline extraction and used them to reinforce TPS.[8] In addition to enhancing both the modulus and tensile strength, the incorporation of LCNFs improved the water barrier properties and reduced water sensitivity compared to neat TPS films.[8] LCNFs extracted from residual oil palm empty fruit bunches were utilized as reinforcement in starch-based biofoams, which resulted in an improvement in the compression resistance of the composite foam and a reduction in water sorption.[9] The marked improvement of water sensitivity and water barrier properties induced by the presence of lignin in LCNF is worth mentioning as highlighted by the work of the group of Yan et al.,[7,8,10] where the addition of 5−10 wt % of LCNF with high amounts of lignin (about 20−23 wt %) contributed to significantly improved thermal and water vapor barrier properties in PLA-based composites. The reduction in water sensitivity brought by LCNF was also achieved in thin-film-based nanocelluloses.[11]

Starch-blended biodegradable polymers (SBBPs) are widely used in various applications, such as food and edible films, as well as flexible and rigid packaging like thermoformed trays and containers. Additionally, they are employed in agriculture as mulching or covering films and materials for plant pots, where TPS was mostly blended with PBAT to produce biodegradable plastics with properties similar to low-density polyethylene (LDPE).[12−14] Motivated by their biodegradability and lower cost, the main factors driving the steady growth of industrial production of starch-blended biodegradable polymers include the lower price and wide availability of starch, coupled with its environmentally friendly nature and ready biodegradability.[15] Due to the significant difference in surface properties, hydrophilic TPS and hydrophobic polyester matrices are entirely immiscible, resulting in heterogeneous materials where the TPS phase is often dispersed within the continuous polyester phase. To enhance the interfacial adhesion between the continuous polyester phase and the dispersed TPS and mitigate the deterioration in mechanical properties arising from the heterogeneous morphology of the polymer blend, a compatibilizer or coupling agent was incorporated.[15,16] Typically, reactive compatibilizers, including maleated polyester and epoxidized polymers such as Joncryl ADR, are considered among the most efficient and widely used in SBBPs.[17,18] Another limitation of SBBPs is the narrow range of TPS content, which rarely exceeds 30 wt % in commercial products. Beyond this content, the pronounced hydrophilicity of TPS, along with its poor mechanical properties, results in materials with low mechanical strength and high water sensitivity and absorption, making them incompatible with the commercial use of SBBP films.[19]

The addition of nanoparticles (NPs) is another approach to modify the microstructure and behavior of polymer blends thanks to their high specific surface (high surface area-to-volume ratio, a wide range of possibilities in surface functionalities, different types of morphology, and the ability to form a network).[20−23] When present in polymer blends, NPs can

(i) act as a reinforcing agent for the continuous or dispersed phase, serving as a barrier against crack propagation;

(ii) induce the formation of a network structure;

(iii) impact the crystallization behavior of the continuous or dispersed phase through their nucleating aptitude;

(iv) alter the compatibility between the two polymer phases if NPs accumulate at the interface;

(v) improve the barrier properties, particularly when NPs are highly impermeable to gases or vapors like water, oxygen, or CO_2, and create tortuous paths for the diffusion of gases.

However, the magnitude of the impact of NPs on polymer blends heavily relies on specific properties of the NPs (chemical composition, size, morphology, and surface chemistry). Therefore, the knowledge of their characteristics is essential to achieve the desired modifications in the behavior of the polymer blend, in terms of mechanical properties, water sensitivity, and processability. Moreover, to mitigate the potential adverse effects of NPs on the environment in biobased biodegradable polymer blends, the use of biobased NPs as additives in polymer blends would be of great benefit. In this sense, only a limited number of studies have explored the incorporation of biobased NPs into PBAT/TPS blends. Silva et al. investigated the effects of adding cellulose nanocrystals (CNCs) at various contents ranging from 0 to 3 wt %, in PBAT/TPS blends with a 75/25 wt % ratio using melt extrusion.[24] However, the study lacked a discussion on the evolution of the mechanical properties of the films, according to the CNC content, and the main focus was on the evolution of the water transmission rate (WVP). This research was subsequently extended to explore the effect of CNCs on the mechanical and rheological properties of PBAT/TPS blends.[25] The increase in CNC content was accompanied by an increase in melt viscosity, positively impacting the mechanical properties of the film with improvements in both tensile modulus and strength. Recently, a PBAT/TPS/lignin blend containing 20, 30, and 40 wt % TPS/lignin filler was prepared by twin-screw extrusion and injection molding.[26] The inclusion of lignin enhanced thermal stability, lowered crystallization temperatures, and increased the hydrophobicity of the composite.

In a previous study, PBAT/TPS blends with a 50/50 wt % ratio containing CNFs at various contents (0−15 wt %, based on TPS) were processed using twin-screw extrusion.[27] The study aimed to assess the influence of CNFs on the microstructure, mechanical properties, melt rheology, and water sorption of PBAT/TPS blend films. The incorporation of CNFs resulted in an enhancement of tensile strength and modulus. However, the water sorption was not reduced. This limitation hindered the possibility of increasing the TPS content beyond 20−30 wt %.

In the present study, LCNFs were initially mixed with TPS and blended with PBAT to fabricate PBAT/TPS/LCNF blends, with TPS and LCNF contents ranging from 30 to 50 wt % and 6 to 10 wt % (based on TPS), respectively. The main goal was to enhance the mechanical properties of the films and reduce the water sensitivity of the PBAT/TPS blends, addressing a key limitation of this category of biodegradable plastics.

https://doi.org/10.1021/acssuschemeng.4c02245
ACS Sustainable Chem. Eng. 2024, 12, 10805−10819

2. EXPERIMENTAL SECTION

2.1. Materials. PBAT (EcoflexF Blend C1200) was acquired from BASF (Germany), with a density ranging from 1.25 to 1.27 g cm^{-3} and a melt flow index of 4 g min^{-1}. Glycerol (G) and maleic acid (MA) were obtained from Sigma-Aldrich. Corn starch was supplied by Roquette Frères S.A (Lestrem, France), and Joncryl ADR 4468 (JC) from BASF was used as a compatibilizer. The raw materials used in the production of LCNFs included discarded components of date palm waste (DPW), such as a blend of leaflets, leaves, and rachis, obtained from the yearly pruning of date palm trees in the oasis region of Gabes, South Tunisia, serving as the biomass feedstock. DPW was milled using a domestic knife mill and sieved at about 5 mm.

2.2. LCNF Preparation. The LCNFs were prepared according to the method reported in our previous work.[28] In brief, the neat milled biomass underwent a hydrothermal treatment at 160 °C for 1 h, followed by a second hydrothermal treatment at 150 °C in the presence of 20% MA (based on DPW) for 1 h, at a solid-to-liquid ratio of 1:10. After multiple washing/filtrations to remove MA, the suspension was disintegrated in a high-pressure homogenizer PANDA Plus 2000 (GEA Niro Soavi, Italy), at 1.5 wt % consistency (3 passes at 300 bar and 3 passes at 600 bar). The resulting LCNFs have a thick gel-like aspect with a brown color.

2.3. PBAT/TPS/LCNF Blend Processing. The processing of PBAT/TPS/LCNF blends involved two distinct stages, using a laboratory-scale twin-screw extruder (TSE, DSM-Xplore15 cm^3 Microextruder). In **stage 1**, TPS/LCNF was prepared by extrusion of the starch, glycerol, and LCNF, as follows. Starch and glycerol (70/30 wt %) were mixed with the appropriate amount of LCNF suspension. The mixture was compounded in the TSE at 100 rpm and 25 °C for 5 min, and the extrusion was pursued by increasing the temperature to 110 °C to ensure the gelatinization of starch. The TPS/LCNF blend was then pelletized and dried in an oven maintained at 70 °C for 24 h. In **stage 2**, TPS/LCNFs and PBAT pellets at different weight ratios were extruded at 150 °C and 120 rpm. The melt blend exits a flat die in the form of a thin film with a rectangular cross-section of 3 × 0.15 mm^2. Figures S1 and S2 illustrate the processing route for PBAT/TPS blends and the visual aspect of the resulting films. A Letsritz 18 MAXX twin-screw extruder was used for pilot test processing, with a screw diameter of D = 18.5 mm and a screw length of 32D (60 cm).

The blend samples will be referred to as PBAT/TPS/LCNF (X/Y/Z), where X, Y, and Z indicate the wt % of PBAT, TPS, and LCNFs, respectively. The wt % of LCNFs (Z) contained in the blend was based on the weight of TPS.

2.4. Blown Extrusion of PBAT/TPS/LCNF Blends. The process of preparing blown films involved drying the PBAT/TPS/LCNF blend granules for 24 h at 70 °C and subsequently feeding them into a pilot extrusion machine equipped with a single-screw film blowing system (screw diameter: 20 mm, length-to-diameter ratio: 28:1) manufactured by SCM20, Lianjiang Machinery, China. Additional information regarding the specific temperature zones and screw speed utilized during the blown extrusion process can be found in Figure S3. The blow-up ratio (BUR) was calculated by eq 1

$$\mathrm{BUR} = \frac{\mathrm{EEF}}{D_d \times 1.569} \tag{1}$$

where EEF represents the edge-to-edge of the film when flat and D_d corresponds to the die diameter.

The draw-down ratio (DDR) is defined as the reduction in thickness of the molten material following the blowing process, and its value is calculated with eq 2

$$\mathrm{DDR} = \frac{D_g}{F_t} \times \frac{1}{\mathrm{BUR}} \tag{2}$$

where D_g and F_t represent the die gap and the thickness of the film, respectively. Table 1 lists the blowing and processing parameters.

2.5. Transmission Electron Microscopy (TEM). Droplets of diluted LCNF suspensions were deposited onto previously glow-discharged carbon-coated copper grids. After negative staining with 2 wt % uranyl acetate, the specimens were allowed to air-dry. In addition, ultrathin (90 nm) cross sections of a 20 μm-thick film of a PBAT/TPS (60/40) blend incorporating 8 wt % LCNFs were prepared with a Leica UC6 ultramicrotome under cryo conditions (−70 °C). The sections were collected on carbon-coated TEM grids and observed at room temperature under low-dose conditions. All specimens were observed with a JEOL JEM 2100-Plus microscope operating at 200 kV. Images and electron diffraction patterns were recorded with a Gatan Rio 16 camera.

Table 1. Blown Extrusion Parameters

blown extrusion settings	metrics
edge-to-edge when flat (EEF)	122 mm
bubble radius (R_b)	39 mm
die diameter (D_d)	45 mm
die gap (D_g)	0.8 mm
film thickness (F_t)	0.035 mm
blow-up ratio (BUR)	1.72
draw-down ratio (DDR)	13.33

2.6. Moisture Sorption. The sample in the form of a film was dried at 80 °C for 24 h and placed in a hermetic container with a controlled degree of relative humidity (RH) kept constant by the presence of a saturated solution of a salt (NaCl for 75% RH, and magnesium nitrate $Mg(NO_3)_2$ for 55% RH). The moisture uptake by the samples was determined by periodical weighting until a constant mass was reached. The moisture absorption was calculated using eq 3

$$\text{moisture sorption (\%)} = \frac{(m_t - m_0)}{(m_0)} \times 100 \tag{3}$$

where m_t and m_0 are the weight of the sample at a given time and the initial weight of dried samples, respectively. Measurements were run in triplicates to ensure reliability.

2.7. Tensile Tests. Tensile tests were conducted at room temperature utilizing an Instron tensile test machine with a cross-head speed of 20 mm min^{-1}. Each composition was subjected to testing with five specimens to ensure statistical reliability. For the blown film, identical parameters were applied to both the extrusion direction (ED) and the transverse direction (TD).

2.8. Dynamic Mechanical Analysis (DMA). Torsion mode DMA experiments were performed using a Perkin-Emer Pyris Diamond DMA from Bruker Instruments (Massachusetts). Temperature scans were executed in the range of −80 to 150 °C, employing a controlled heating rate of 2 °C min^{-1}, a frequency set at 2 Hz, and an oscillation amplitude of 15 μm. The samples with dimensions approximately 15 mm in length, 5 mm in width, and 0.25 mm in thickness were subjected to the analysis.

2.9. Scanning Electron Microscopy (SEM). The extruded samples were fractured after quenching in liquid nitrogen. To better characterize the shape and size of the dispersed phases, the surface of the cryo-fractured sections was etched in 1 M HCl (3 h at 50 °C) to dissolve the TPS phase. After extensive washing with water, the specimens were air-dried, coated with Au/Pd in a Safematic CCU-010-HV sputter-coater, and observed in secondary electron mode in a Thermo Scientific Quanta 250 scanning electron microscope equipped with a field-emission gun and operating at 2.5 kV.

2.10. Molten State Rheological Properties. The rheological properties of molten blends comprising TPS/LCNFs and PBAT/TPS/LCNFs were examined using a controlled rate dynamic mechanical rheometer (ARES-G2 from TA Instruments). The analysis employed a plate−plate geometry with a 25 mm diameter and a 1-mm gap. Measurements of the storage modulus G', loss modulus G'', and complex viscosity η^* of the blended films were conducted at a temperature of 160 °C over a frequency range of 0.01−10 Hz. Before each measurement, the linear viscoelastic region was determined through an amplitude sweep within the deformation

https://doi.org/10.1021/acssuschemeng.4c02245
ACS Sustainable Chem. Eng. 2024, 12, 10805−10819

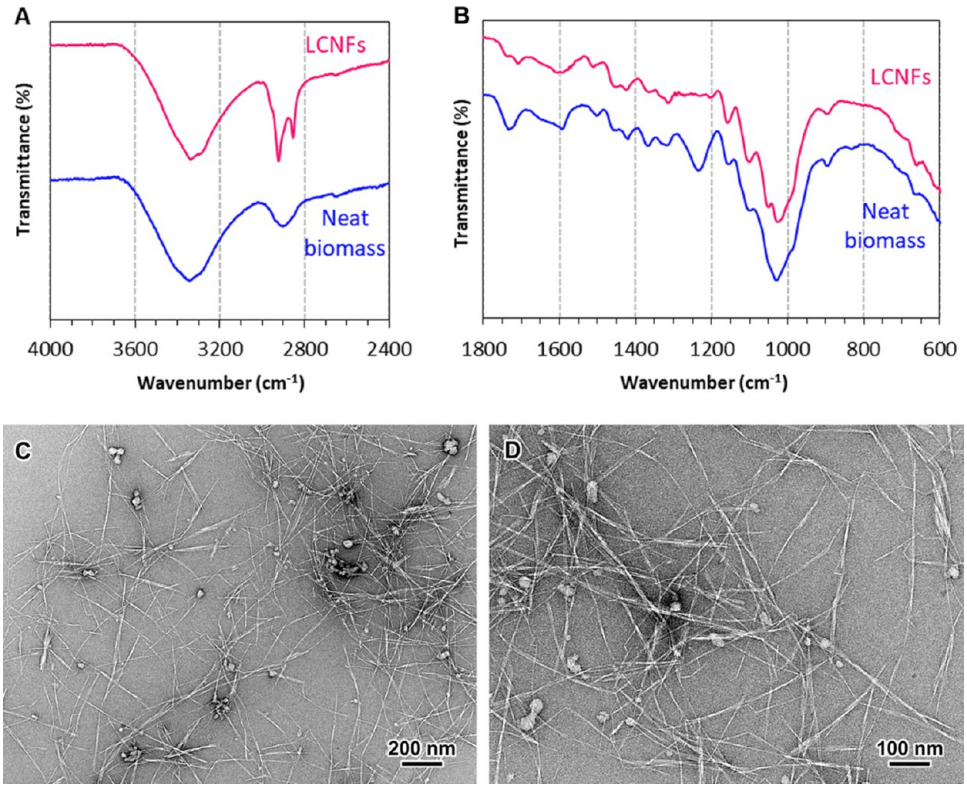

Figure 1. (A, B) FTIR spectra of neat biomass used for the preparation of LCNFs and that of the corresponding LCNFs and (C, D) TEM images of a negatively stained preparation from a dilute suspension of LCNFs.

range of 0.1−100% at 1 Hz to precisely identify the linear viscoelastic region.

2.11. Water Contact Angle Measurement (WCA). The water contact angle (WCA) of the nanocomposite films was determined utilizing an OCA 15 Drop Shape Analyzer from Dataphysics, which was equipped with a CCD camera operating at an acquisition rate of 50 images per second and the OCA analysis software. A 5 μL droplet of distilled water was deposited onto the film surfaces, and the average WCA value was computed based on measurements from at least three specimens.

2.12. X-Ray Diffraction (XRD). Strips of nanocomposites were cut, and XRD patterns were recorded in vacuum using the Ni-filtered Cu Kα radiation (λ = 0.1542 nm) produced with a Philips PW3630 generator operating at 30 mV and 20 mA. The patterns were recorded on Fujifilm imaging plates, read with a Fujifilm BAS 1800II bioanalyzer, and rotationally averaged to obtain diffraction profiles that were normalized to the total amount of material.

2.13. Fourier-Transform Infrared Spectroscopy. FTIR spectroscopy was conducted using a PerkinElmer FTIR Spectrum 100, equipped with a single-reflection diamond crystal plate ATR MIR accessory. The data were collected with a resolution of 4 cm^{-1} across the range of 500 to 4000 cm^{-1}.

2.14. Disintegration of the Films in Vegetable Compost. Film fragments (4 cm × 4 cm) were buried at about 5 cm in depth in the soil composed of vegetable compost at a temperature of 58 °C. Water was sprayed once a day to sustain the moisture of the compost. Samples were taken at different times and photographed for visual tracking of the films.

2.15. Biodegradation in Water by the Biochemical Oxygen Demand (BOD) Method. The biodegradation of the PBAT/TPS/LCNF composites in water was assessed by respirometry tests (VELP-Scientifica) to measure oxygen consumption over time. The respirometer was composed of a 6 × 1000 mL individual BOD testing bottle containing a mineral solution (0.1 g L^{-1} of KH_2PO_4/0.021 g L^{-1} of K_2HPO_4/0.35 g L^{-1} of Na_2HPO_4) into which 20 mg of polymer film was soaked. For some bottles, the lipase enzyme Novozyme 51032 was added (100 U mL^{-1}) to evaluate the effect of the presence of the enzyme on the degradation process. Each bottle was continually stirred to equilibrate concentrations and incorporate oxygen into the nutrient medium. During respirometry tests, KOH pellets were placed on a holder inside the bottle to adsorb the released carbon dioxide. The biodegradation test was conducted at 20 °C under stirring for 30 days. The observed volume of oxygen consumption (BOD_{test}) was corrected by subtracting the volume of oxygen consumption of the blank (BOD_{blank}). The theoretical oxygen demand (ThOD) was calculated based on the structural composition of the composites, assuming that the degraded products were completely mineralized to CO_2. The biodegradation percentage (%) was calculated using as follows

$$\text{biodegradation (\%)} = \frac{BOD_{test} - BOD_{blank}}{ThOD} \quad (4)$$

3. RESULTS AND DISCUSSION

3.1. LCNF Characterization. The LCNFs with a high lignin content were produced through hydrothermal treatment of raw date palm waste at 150 °C, with maleic anhydride (MA) as a pretreatment. Then, the fibers were disintegrated using a high-pressure homogenizer (HPH), following the procedure detailed in our previous study.[28] The merit of this approach lies in utilizing raw biomass directly as the starting material for LCNF production, eliminating the necessity for any prior partial delignification. Apart from sustainability considerations, this approach preserves a significant portion of the chemical components, specifically, hemicellulose, cellulose, and lignin, in the LCNFs. This resulted in improved thermal stability, reduced hydrophilicity due to the presence of lignin, and a higher yield in nanoscale material.

The LCNF fraction contained 62 wt % cellulose, 15 wt % hemicelluloses, 20 wt % lignin, and 3 wt % ashes. The XRD

https://doi.org/10.1021/acssuschemeng.4c02245
ACS Sustainable Chem. Eng. 2024, 12, 10805−10819

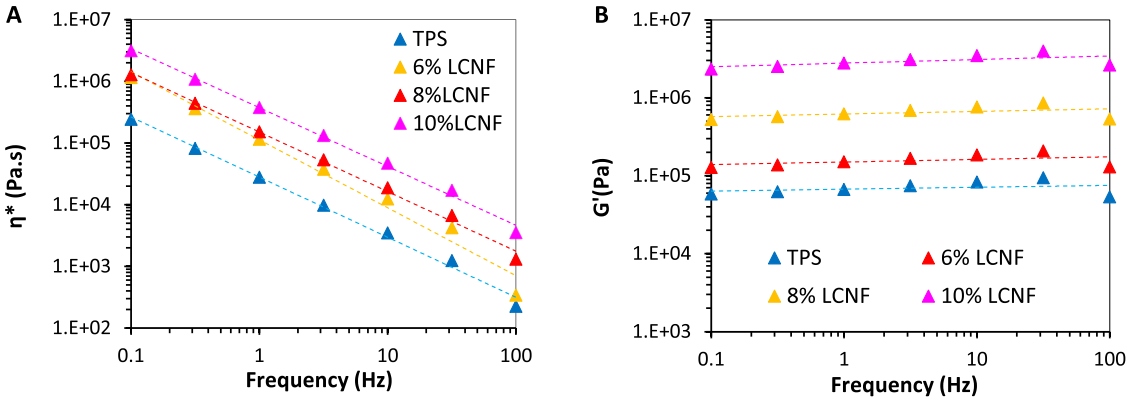

Figure 2. Complex viscosity η^* (A) and storage modulus G' (B) at 150 °C of TPS with different LCNF contents.

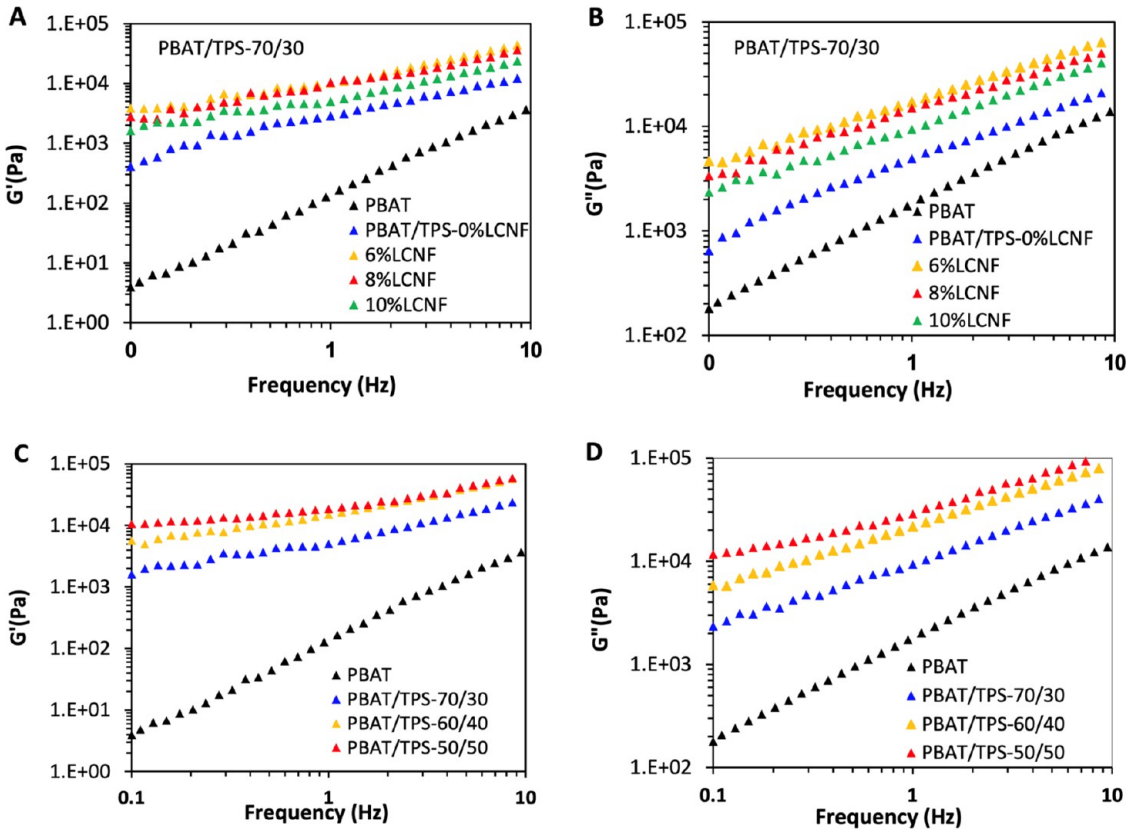

Figure 3. (A, C) Storage modulus (G') and (B, D) loss modulus (G'') vs frequencies (f) at 160 °C of neat PBAT, and PBAT/TPS at different PBAT/TPS ratios and LCNF contents: (A and B) PBAT/TPS 70/30 and LCNFs from 0 to 10 wt % and (C, D) PBAT/TPS from 70/30 to 50/50 wt % and LCNFs = 10 wt %.

profile of the LCNFs (Figure S3) showed typical diffraction peaks of cellulose I at 2θ = 16.1, 22.3, and 34.8° corresponding to the overlapping ($1\bar{1}0$) and (110), (200), and (004) crystal planes, respectively (indexes of allomorph Iβ).

The FTIR spectra of the neat biomass and LCNFs reflected the typical bands in lignocellulosic biomass originating from cellulose, hemicellulose, and lignin (Figure 1A,B). The typical cellulose bands can be seen at 897 cm^{-1} (ν_{C-H}), 1025 and 1050 cm^{-1} (ν_{C-O} s), 1115 and 1155 cm^{-1} (ν_{C-O-C} ring-stretching), 1200 and 1230 cm^{-1} (δ_{C-OH}), 1265 cm^{-1} (δ_{C-H}), 1314 cm^{-1} (ω_{C-H2}), 1332 cm^{-1} (δ_{C-OH}), 1365 cm^{-1} (δ_{C-H}), and 1420 cm^{-1} (δ_{C-H2}). The hemicellulose bands were visible at 1450 cm^{-1} (δ_{C-H}), 1610 cm^{-1} (ν_{COO-} asy), and 1740 cm^{-1} ($\nu_{C=O}$).[29] The peak values at 1325 cm^{-1} (guaiacyl-syringyl-ring), 1500 cm^{-1} (aromatic skeletal vibrations), 1590 cm^{-1} (aromatic skeletal vibrations and C=O stretching), and 1705 cm^{-1} (C=O stretching in ketones, conjugated aldehydes, and carboxylic acids) were characteristic peaks of lignin.[30] The close similarity between the FTIR spectrum of neat biomass and LCNFs confirmed that the main component of the neat biomass was persistent in the LCNFs, which is the main merit of the present approach to the production of LCNFs, as discussed in details in our previous work.[28] Overall, the persistence of lignin contributed to reducing the hydrophilicity of LCNFs.

The TEM images of negatively stained LCNFs showed that the nanofibrils, whether isolated or in bundles, were generally kinked and formed tangled networks (Figure 1C,D). Individual

https://doi.org/10.1021/acssuschemeng.4c02245
ACS Sustainable Chem. Eng. 2024, 12, 10805−10819

cellulose nanofibrils were longer than 1 μm, with widths between 3 and 5 nm. Spheroidal nanoparticles measuring 20−50 nm in size were noted, along with larger aggregates, which correspond presumably to lignin NPs released from the fiber during the HPH treatment. The lignin NPs appeared to be well dispersed within the nanocellulose networks.

3.2. Melt Rheology of TPS/LCNF Mixtures and PBAT/TPS/LCNF Blends. As illustrated in Figure 2A, the melt viscosity η^* of TPS continuously increased with increasing LCNF content, showing a 10-fold increment at 10 wt % LCNFs compared to pure TPS. The same trend was observed for storage and loss moduli (G' and G''), indicating a stiffening of the TPS with the addition of LCNFs (Figure 2B). This effect was expected and might be explained by the formation of interconnected network-like structures in the starch/LCNFs composites, held by hydrogen bonding between CNFs and starch chains, and restrict the flowing of macromolecular chains in the melt. A similar effect was reported in the presence of other classes of hydrophilic polymer matrices such as poly(vinyl alcohol) (PVA), polyethylene glycol (PEG), or poly vinylpyrrolidone (PVP), when CNCs or CNFs were added to these polymers. Thanks to their high aspect ratio and high interaction of CNFs with starch, through hydrogen bonding, the presence of CNFs restrained the flowing of plasticized starch chains in the melt.[31]

The melt rheology of the PBAT/TPS blends with varying LCNF contents was studied at 150 °C through sweep measurement of the storage modulus G', loss modulus G'', and complex viscosity η^* as a function of frequency f in the linear domain (Figure 3). The neat PBAT matrix exhibited a liquid-like character with G'' significantly higher than G' (more than 1 order of magnitude over the whole frequencies studied). A power-law relation over the frequency domain with $G' \sim f^{1.5}$ and $G'' \sim f^{0.88}$, which is close to the theoretical exponent values of 2 for G' and 1 for G''. The deviation observed is likely due to polydispersity in the molecular weight of the commercial PBAT used. The complex viscosity η^* of PBAT is characterized by short a Newtonian plateau at low shear rates, followed by a shear-thinning behavior over 0.2 Hz (Figure S3).

In the PBAT/TPS blends, an upward shift of the G' and G'' plots was observed, and the ratio between G'' and G' markedly decreased, shifting from 15 for neat PBAT to about 1.5 for PBAT/TPS at f = 1 Hz. This significant change in the viscoelastic properties of the PBAT/TPS blend indicates an increasing melt stiffness with the addition of TPS. Additionally, the trace of G' and G'' lies between those of neat PBAT and TPS, as expected for a polymer blend with a dispersed morphology and good interfacial adhesion between the two phases. In this later morphology, the melt rheology often represents a combination of the rheology of the individual components weighted by their volume fraction in such cases.[32] In the presence of LCNFs, at the same PBAT/TPS ratio, both G' and G'' demonstrated a higher level compared to the blend without LCNFs. This effect results from the increased melt stiffness of the TPS with the addition of LCNFs, as shown in Figure 3, where a consistent upward shift in G' and G'' is evident with increasing LCNF content.

At low frequencies, a positive deviation is observed in G', arising from an additional contribution resulting from the shape relaxation of the droplets of the dispersed phase, giving rise to an additional viscoelastic contribution known as the Palierne effect.[33]

3.3. Structure and Morphology of the PBAT/TPS/LCNF Blends. The semicrystalline structure of TPS, PBAT, and PBAT/TPS blends (Figure 4) was analyzed by XRD. The

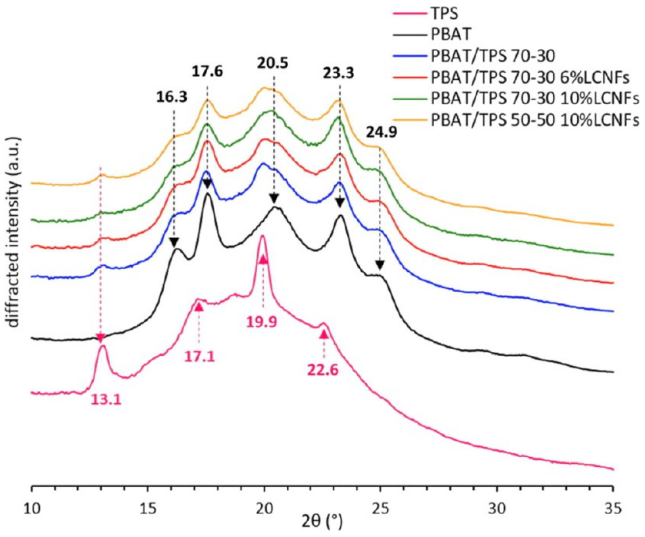

Figure 4. XRD profiles (B) of TPS, PBAT, and PBAT/TPS films with different LCNF contents.

profile of PBAT contained diffraction peaks at 2θ = 16.3, 17.6, 20.5, 23.3, and 24.9°, consistent with literature data.[34] TPS showed peaks at 2θ = 13.1, 17.1, 19.9, and 22.6°. These peaks did not correspond to the A-type structure of the parent native starch granules but rather indicated the presence of a $V6_I$ inclusion complex (also referred to as V_H) likely formed between amylose and the small fraction of endogenous lipids present in corn starch granules.[35] The formation of a V-type allomorph has previously been documented in studies describing the processing of TPS from cereal starch sources.[36] Since the amount of lipids was low, the major part of the TPS phase was thus amorphous and only contributed to the background scattering. The profiles of PBAT/TPS/LCNF blends were superpositions of those from PBAT and TPS. It was not possible to detect the peaks corresponding to the cellulose fraction of LCNFs, likely because the LCNF content was small, and the main peaks of cellulose overlapped with peaks of the V-type allomorph (Figure S4). However, incorporating LCNFs did not influence the crystallization properties of both the TPS and PBAT phases.

Cross-sectional surfaces of cryo-fractured PBAT/TPS/LCNF films subjected to an etching treatment in 1 M HCl to selectively dissolve the TPS phase were observed by SEM (Figure 5). The porosity was assumed to result from the etching of the TPS phase, which is more sensitive to acid degradation. At the same PBAT/TPS ratio (70/30), the increase in LCNF content significantly influenced the morphology of PBAT/TPS blends. In the absence of LCNFs, the TPS phase was homogeneously distributed in the form of 4−5 μm spheroidal nodules with a relatively narrow distribution. However, with the addition of LCNFs, the particle size of the dispersed TPS phase increased, becoming larger and much broader with large and irregular particles as the LCNF content increased, with a mean size around 7, 14, and 20 μm, for LCNF contents of 6, 8, and 10 wt %, respectively (Figure S5). This result was unexpected, given the substantial improvement in mechanical properties observed

https://doi.org/10.1021/acssuschemeng.4c02245
ACS Sustainable Chem. Eng. 2024, 12, 10805−10819

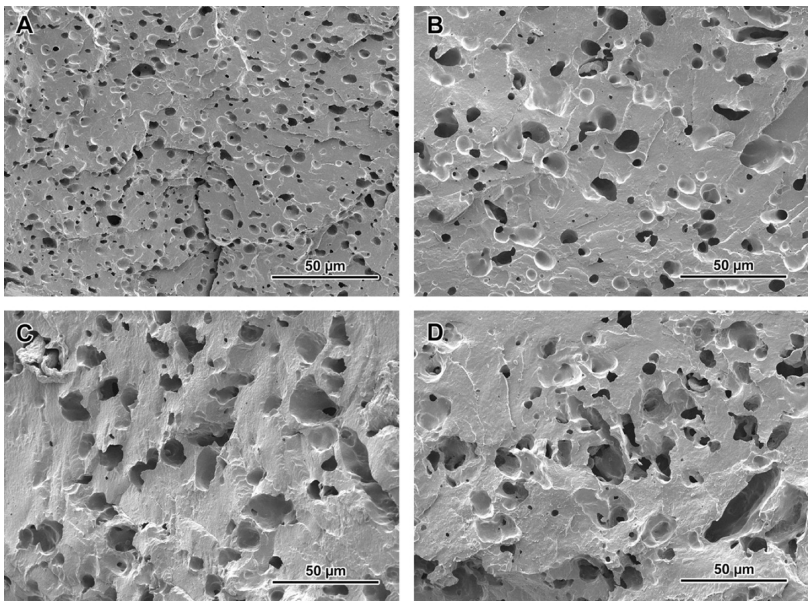

Figure 5. SEM micrographs of cryogenically fractured surfaces for PBAT/TPS (70/30) at different LCNF contents: (A) 0 wt %, (B) 6 wt %, (C) 8 wt %, and (D) 10 wt %. A treatment in 1 M HCl was performed to etch away the TPS phase.

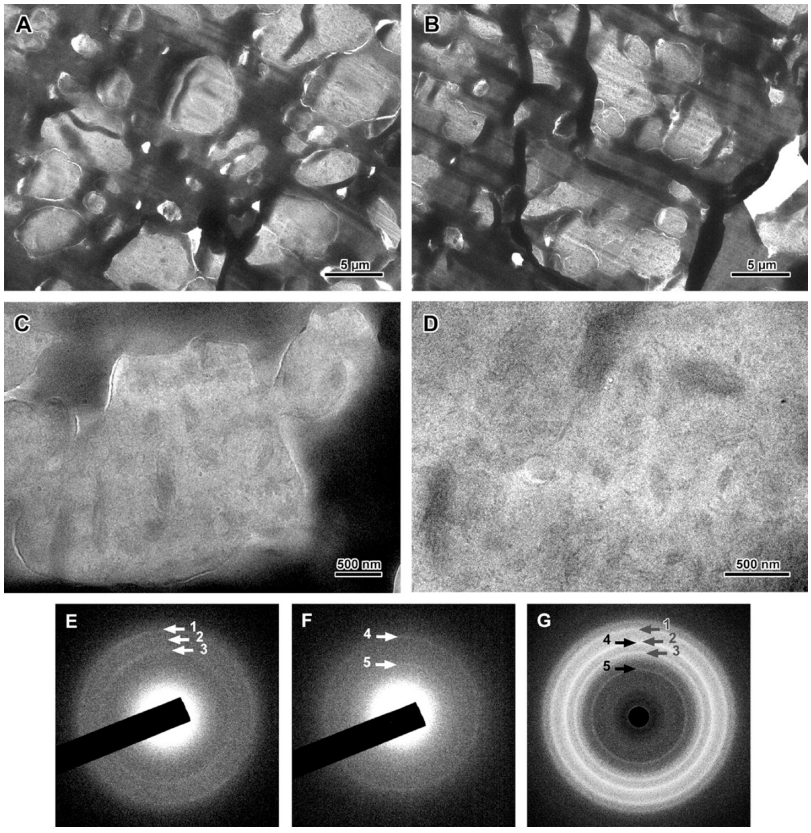

Figure 6. (A–D) TEM images of ultrathin cross sections of a PBAT/TPS (60/40) film with 8 wt % LCNFs. The dark regions would correspond to the PBAT matrix while the clear regions would be the TPS nodules. At higher magnification (C, D) of TPS regions, the darker fibrillar objects would correspond to dispersed LCNF. (E, F) Electron diffraction patterns recorded from the dark (E) and clear (F) regions. The diffraction rings were numbered to facilitate the comparison with the XRD pattern collected from the parent blend film: 1, 2, and 3 belong to the PBAT phase while 4 and 5 would correspond to the $V6_I$ inclusion complex fraction in the TPS phase (also identified in the XRD profiles in Figure 4) (G).

with the addition of LCNFs to TPS. We presumed that the morphological evolution was influenced by the melt rheology of the TPS phase in the presence of LCNFs. Indeed, the increase in the melt viscosity of TPS in the presence of LCNF, highlighted in Figure 2, induced a greater resistance to the breakup of dispersed polymer droplets, thus reducing the extent of particle coalescence during processing. The key role of the melt viscosity of the dispersed phase in controlling the

https://doi.org/10.1021/acssuschemeng.4c02245
ACS Sustainable Chem. Eng. 2024, 12, 10805−10819

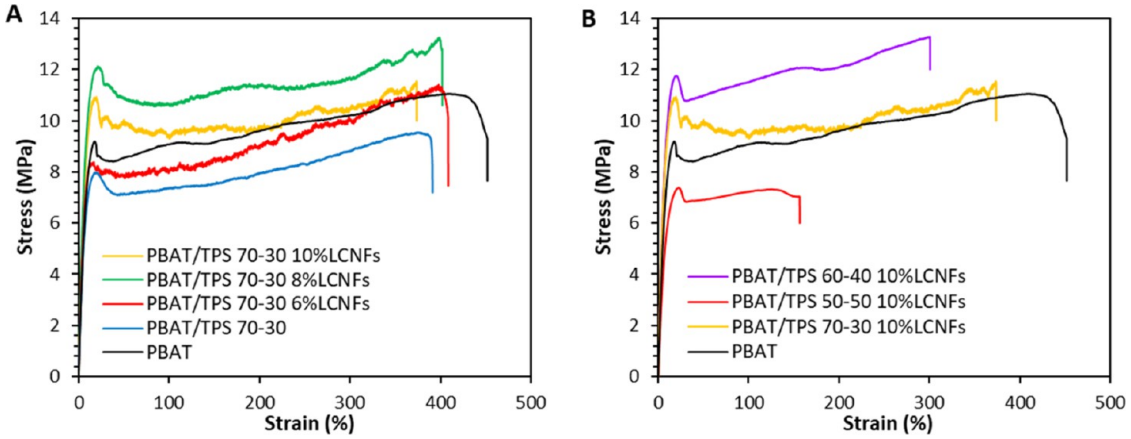

Figure 7. Stress−strain curves for PBAT/TPS at different content in LCNFs, (A) PBAT/TPS at 70/30 ratio and (B) at different PBAT/TPS ratios and 10 wt % LCNF loading.

morphology of the polymer blends has been highlighted in the literature.[37,38] The possible effect of evolution in the interfacial properties following the addition of LCNFs may also contribute to the change in the morphology of the polymer blend. However, this effect is mitigated by the addition of the reactive coupling agent, which enhances interfacial adhesion between PBAT and TPS through the reaction of the oxirane ring between the hydroxyl groups of TPS and PBAT. Nevertheless, the hydrophobic nature of lignin suggests the possibility of lignin NPs accumulating at the PBAT/TPS interface. With increasing the TPS content and keeping constant the LCNF content, the nodular morphology of the TPS phase was preserved up to 50 wt % TPS, with an increase in the size of the nodules with increasing TPS content, as shown in Figure S6.

TEM images of ultrathin cryosections of a PBAT/TPS 60/40 film incorporating 8 wt % LCNFs are shown in Figure 6A,B. They confirmed the heterogeneous microstructure of the material. Although the film was microtomed at a temperature far below the T_g of both PBAT and TPS, folding was observed, presumably mostly in the PBAT matrix that appeared as darker regions. Indeed, despite the high radiation sensitivity of the specimen, the electron diffraction pattern recorded on a dark region of the section contained three rings that corresponded to reflections identified in the XRD pattern of PBAT (Figures 4 and 6E,G). The pattern recorded on a clear region contained only two rings that correspond to reflections of the $V6_I$ inclusion complexes in the TPS phase that were also detected in the XRD pattern (Figures 4 and 6F,G).[35] High-magnification images of TPS regions showed the presence of fairly well-dispersed fibrillar elements that presumably corresponded to fragments of sectioned LCNFs. In addition, the contrast of these fragments rapidly decreased due to the fast damage of the cellulose nanofibrils under the electron beam. In line with the XRD results, it was not possible to record the diffraction rings from cellulose by electron diffraction, likely due to the small LCNF fraction and its good dispersion within the TPS nodules.

Unfortunately, from TEM images, it is not possible to have an accurate indication of the location of lignin NPs, owing to the amorphous character of lignin, their small size, and density close to that of the other constituents. The better visibility of cellulose nanofibrils, despite their density similar to that of starch, is due to their crystallinity which generates a contrast.

3.4. Mechanical Properties of the PBAT/TPS/LCNF Blends. The mechanical properties of the PBAT/TPS/LCNF blends were assessed through tensile tests at 20 °C and DMA measurements over a wide temperature range from −80 to 120 °C (Figure 7A,B). The neat PBAT film exhibited a tensile modulus (E) of approximately 10^5 MPa, a yield strength (YS) of around 9 MPa, and a strain at break (SB) exceeding 400%, indicative of a highly ductile polymer with mechanical properties close to those of LDPE. These data agree with those from the literature.[39] The addition of TPS to PBAT resulted in a reduction in YS and SB, as expected due to the heterogeneous microstructure of the blend with the TPS phase being dispersed in the PBAT matrix. This induces a stress concentration effect that promotes the premature breaking of the film. The addition of the coupling agent contributed to improving the interfacial adhesion between PBAT and TPS, facilitating stress transfer between the two phases and enhancing the strength of the film. This improvement in interfacial adhesion explains the superior mechanical properties of the PBAT/TPS blends in the presence of the coupling agent Joncryl (JC).

Subsequently, all blends incorporating LCNFs were processed in the presence of JC to enhance interfacial adhesion. The addition of LCNFs, up to 10 wt %, to the blend containing 30 wt % TPS (PBAT/TPS 70/30) had a positive effect on both the yield strength (YS) and the tensile modulus (E), without compromising the ductility of the film as indicated by the high strain at break (SB) that remained over 300%. At 6, 8, and 10% LCNFs, the increase in YS/E compared to blends without LCNFs was 14/50, 37/100, and 45/115%, respectively.

A similar trend was observed in PBAT/TPS (60/40), where the addition of 10 wt % LCNFs resulted in an enhancement of YS/E by about 105/140% compared to the same composition without LCNFs. This implies that the addition of LCNFs to TPS helped mitigate the negative impact of the presence of TPS in the PBAT matrix. Up to a content of 40 wt % TPS, the resulting blend containing 10 wt % LCNFs demonstrated even better strength and stiffness than the neat PBAT matrix, without compromising the ductility of the blend, a crucial property for which PBAT was originally developed. This means that despite the increase in size of the TPS nodules in the presence of LCNFs that would impart the strength of the blend, the inclusion of LCNFs had a beneficial effect on the

https://doi.org/10.1021/acssuschemeng.4c02245
ACS Sustainable Chem. Eng. 2024, 12, 10805−10819

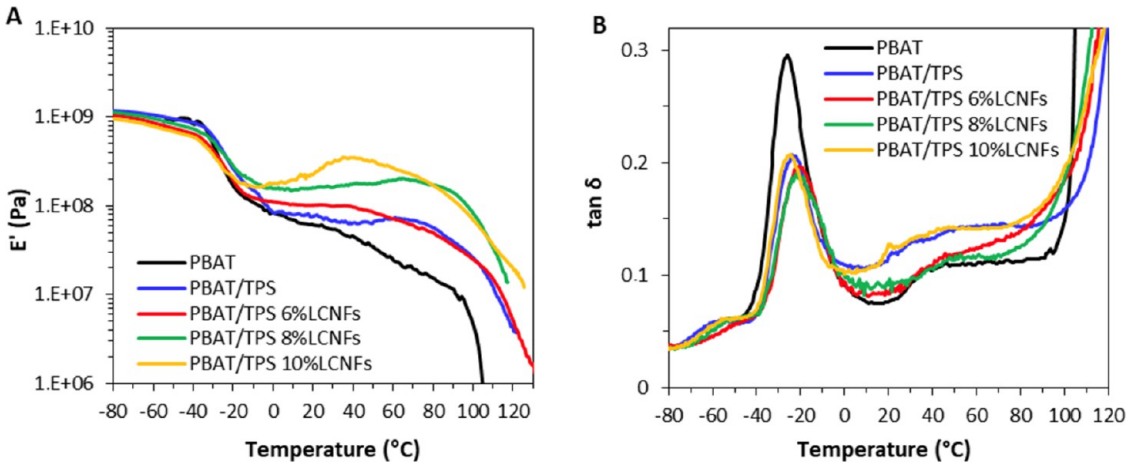

Figure 8. (A) Variation of storage modulus E' and (B) tan δ with temperature for neat PBAT and PBAT/TPS blends at different LCNF contents.

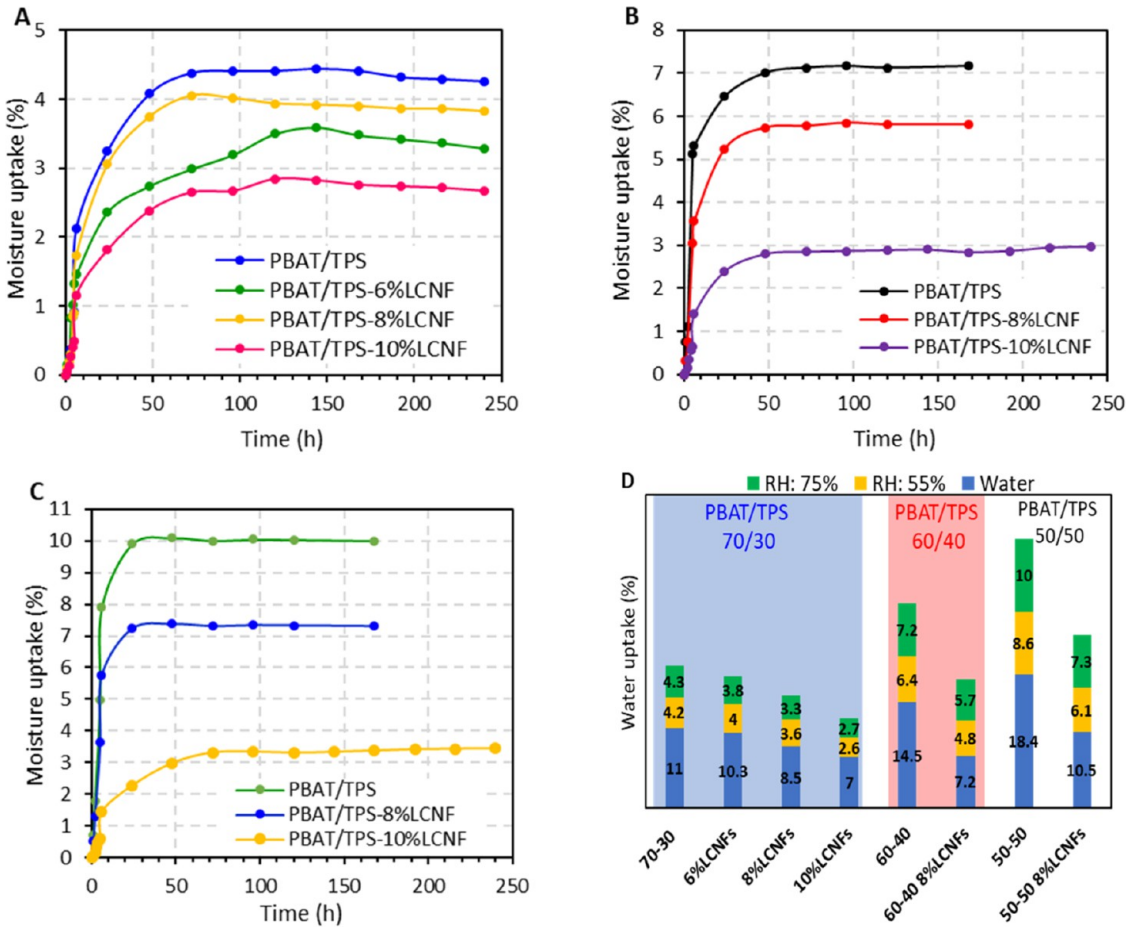

Figure 9. Moisture uptake vs time for PBAT/TPS blends at different ratios and LCNF contents: (A) PBAT/TPS 70/30, (B) PBAT/TPS 60/40, (C) PBAT/TPS 50/50 at different LCNF contents, and (D) compilation of maximum moisture sorption at different PBAT/TPS ratios and LCNF contents. The water sorption under immersion conditions was also included (in blue).

strength of the PBAT/TPS blend, achieving better YS than neat PBAT, even at a TPS content as high as 40 or 50 wt %. This effect was presumably the consequence of the reinforcing effect of CNFs in the TPS phase, which would have a beneficial effect on the US of the PBAT/TPS blends. Indeed, for polymer blends, and when the interfacial adhesion between the two phases was achieved both phases would contribute to the rheological and mechanical properties of the blend in a kind of mixing rule trend. The beneficial effect of the inclusion of CNCs and CNFs in PBAT/TPS blends was also highlighted in the literature.[26,27]

The DMA analysis aimed at assessing the evolution of the storage modulus (E′) reflecting stiffness with temperature and highlight different transitions within the polymer blends (Figure 8A,B). Figure 8A presents the evolution of the storage modulus (E') and tan δ with temperature for the PBAT/TPS

https://doi.org/10.1021/acssuschemeng.4c02245
ACS Sustainable Chem. Eng. 2024, 12, 10805−10819

blends with varying LCNF contents. In the neat PBAT matrix, an abrupt drop in E' by more than a decade at −40 to −20 °C was observed, accompanied by a maximum in the tan δ plot, attributed to the glass transition (T_g) of the soft polybutylene adipate segment of PBAT. A second decay in E' was noted above 40 °C, related to the T_g of the polybutylene terephthalate segment, and over 100 °C, the melting of PBAT resulted in a sharp drop in E'.

For the PBAT/TPS blends, the E' plot exhibited similar features, but the second decay in E' was no longer visible, and the rubbery plateau expanded up to the melting of PBAT. Another transition in the tan δ plot appeared around −60 °C, attributed to the T_g of the TPS phase (Figure 8B).[40]

Incorporating LCNFs resulted in an upward shift of the rubbery plateau with increasing LCNF content, which indicates an enhanced stiffness in the rubbery domain for the PBAT/TPS blend. This observation aligns with the tensile test results, which demonstrated an increase in tensile modulus at 25 °C. Notably, no alteration in the position of the maximum in the tan δ plot was observed, indicating that the addition of LCNFs did not affect the mobility of the macromolecular chains of PBAT or TPS.

3.6. Moisture Uptake. The moisture sorption vs time at 75 and 55% RH for PBAT/TPS blends at different PBAT/TPS ratios and LCNF content is depicted in Figure 9. In all compositions, water sorption steadily increased with time, leveling off after about 3 days at a saturation plateau (M_{max}), representing the equilibrium water sorption. Figure 9 shows that M_{max} varied according to the RH, PBAT/TPS ratio, and LCNF content. An increase in RH and TPS content resulted in a higher M_{max}, as expected, due to the highly hydrophilic nature of TPS, contributing to increasing the water sorption in polyester/TPS blends. Despite the hydrophobic nature of the PBAT matrix, acting as a barrier against the diffusion of water molecules, the content of TPS should not exceed 30 wt % to ensure its effective encapsulation within the PBAT matrix and to keep moisture sorption as low as possible. This justifies that in most commercial PBAT/TPS blends, the TPS content did not exceed 25−30 wt %. Over this level, the moisture sorption at high RH increased by over 5%, which adversely affected the mechanical properties of the blend. Presently, it can be seen that the inclusion of LCNFs over 8 wt % contributed to mitigating the water sensitivity of the PBAT/TPS blends, allowing an increase in TPS content beyond the conventional range of 20−30 wt % adopted in polyester/TPS blends. For instance, at 75% RH, the M_{max} for PBAT/TPS 70/30 wt % decreased from 4.4% in the absence of LCNFs to about 2.7% in the presence of 10 wt % LCNFs, corresponding to a reduction of more than 40% compared to the neat PBAT/TPS blend. Even for a blend composition with higher TPS content (40 and 50 wt %), a significant decrease in moisture sorption was observed (Figure 9D). At 40 wt % TPS, M_{max} decreased from 7 to 3% in the presence of 10 wt % LCNFs, and at 50 wt % TPS, it decreased from 10 to about 3.3%.

The beneficial effect of LCNF addition on moisture sorption is likely due to the presence of around 20 wt % lignin, which contributes to reducing the hydrophilicity of the TPS phase, thanks to the hydrophobic character of lignin. This is supported by a significant change in the contact angle of TPS without LCNFs compared to TPS with 10 wt % LCNFs, where the water contact angle increases from about 13° for neat TPS to more than 80° in TPS containing 10 wt % LCNFs (Figure S7). It is worth mentioning that the reduction in water uptake induced by the addition of LCNFs was even observed under water immersion conditions, as shown in Figure S8. For instance, the water uptake of PBAT/TPS 60/40% film decreased from 14.5% in the absence of LCNFs to around 7% when 8% LCNFs were included in the blend.

The substantial reduction in moisture sorption of PBAT/TPS blends is of great benefit for biodegradable plastics based on polyester/TPS blends, as it has two main effects: (i) a cost reduction of the biodegradable plastic, as TPS is much less expensive than polyester, and (ii) an acceleration of the biodegradation tendency, especially with less biodegradable polyesters like PLA, as the TPS phase is more sensitive to biodegradation due to the presence of starch.

3.7. Pilot-Scale Production of Thin PBAT/TPS/LCNF Films Using Blown Extrusion. Considering that most of the applications for PBAT/TPS blends are intended for producing thin compostable films, such as those used in biodegradable bags or sustainable agricultural applications like greenhouses or mulching films, pilot test experiments were conducted to produce thin films through blown-film extrusion using PBAT/TPS/LCNF blends. The primary objective was to assess whether the presence of LCNFs affects the processing of the biodegradable plastic during film blowing and to evaluate the properties of the resulting films. Three compositions were tested, namely PBAT/TPS 60/40, PBAT/TPS 60/40−8% LCNF, and PBAT/TPS 50/50−8%LCNF. For each composition, LCNFs were mixed with TPS during the processing of TPS by twin-screw extrusion (TSE), and then PBAT/TPS/LCNFs pellets were produced by melt-blending PBAT with TPS/LCNFs using the same TSE. The pellets were fed into a single-screw extruder equipped with a film blow unit operating under the conditions reported in Table 1.

The blowing of the three compositions was successfully carried out, even for the blend containing 50 wt % TPS, resulting in a stable bubble with a tubular shape similar to that of neat PBAT-blown film. Photos illustrating the blown extrusion process in the pilot are presented in Figure 10. Given the high sensitivity of blown extrusion processing to the presence of particles within the film that may act as defects, leading to premature bubble breaking, this result is highly encouraging. It further supports the effective dispersion of LCNFs within the PBAT/TPS blends, likely within the TPS phase, as confirmed by TEM images of cross sections of the film (Figure 6). Additionally, considering the crucial role of melt rheology properties in the success of blown extrusion,[3] the stability of the bubble for the PBAT/TPS/LCNF blends may be attributed to the increased melt elasticity (G') and melt viscosity of the blend when LCNFs were added, enhancing the melt strength during the blowing process and preventing the bubble from collapsing.

The mechanical data for the films produced by blown extrusion are summarized in Table 2, including data for neat PBAT and PBAT/TPS blends containing 8 wt % LCNFs (Figure 11). For all films, the mechanical properties of the blown film were higher in the extrusion direction (ED) compared to the transverse direction (TD) due to the preferential orientation of the polymer macromolecules along the flow direction.[19] Interestingly, the PBAT/TPS (60/40) film containing 8 wt % LCNFs demonstrated higher ultimate strength (US), strength at break, and tensile modulus than the film processed without LCNFs, at a similar PBAT/TPS proportion. The same observation applies to the PBAT/TPS (50/50) composition, consistent with results obtained for

https://doi.org/10.1021/acssuschemeng.4c02245
ACS Sustainable Chem. Eng. 2024, 12, 10805−10819

Figure 10. Photos showing the production of thin film by blown-film extrusion from PBAT/TPS 60/40 blends without LCNFs (A, B) and with 8 wt % LCNFs (C, D).

extruded films using a flat die and discussed in Section 3.2. The PBAT/TPS (60/40) film containing 8 wt % LCNFs exhibits nearly the same US and strain at break (SB) as neat PBAT, and a higher tensile modulus, without compromising the elongation at break. Even the PBAT/TPS (50/50) blend containing 8 wt % LCNFs achieves mechanical properties nearly similar to the PBAT/TPS (60/40) blend. Once again, the addition of LCNFs allowed the incorporation of a higher content of the less expensive TPS constituent, which is highly beneficial for cost considerations and increases the biobased content.

3.8. Disintegration in Soil. A qualitative evaluation of the biodegradation of PBAT/TPS/LCNF blends was conducted by inspecting the disintegration capability of the film under burial conditions in the soil at a temperature of 58 °C. Figure 12 compiles photos of the film's appearance at different burial times. Film fragmentation started after 4 weeks, and nearly complete disintegration was achieved within 8 weeks. This complete disintegration is likely due to the biodegradable nature of PBAT and the inclusion of TPS, which accelerated the biodegradation process, thanks to the high sensitivity of starch to biological degradation upon contact with humid soil.[14] The presence of LCNFs did not appear to alter the susceptibility and readiness of PBAT/TPS blends to biodegradation. While more accurate standard tests for biodegradation, such as monitoring the release of CO_2 overtime at 58 °C under aerobic conditions, should be conducted, the disintegration tests under burial is qualitative and provides a simple method to assess the susceptibility of plastic to biodegradation, as disintegration into fragments is the initial phase of plastic degradation.[41]

3.9. Biodegradation in Aquatic Medium. The biodegradation by immersion in water was also assessed by BOD measurement. This reliable test is easily implemented to simulate different conditions and medium compositions. Figure 13 illustrates the biodegradability of thin PBAT, PBAT/TPS 60/40, and PBAT/TPS 60/40 with 8 wt % LCNFs films in aqueous medium containing enzyme over 30 days. The progressive consumption of O_2 with time for all samples tested indicates the occurrence of biological biodegradation in water. It is worth mentioning that no evolution in O_2 consumption was observed in the control test without PBAT blend film or with a sample of polyethylene (PE) thin film. Unlike in another sample, a lag phase of about 3 days between the introduction of the microorganisms in the medium and the onset of detectable microbial degradation was observed. The presence of the enzyme significantly accelerates the biodegradation kinetics and extent. For instance, for the PBAT/TPS (60/40), the degradation extent after 30 days was about 15% in the absence of the lipase enzyme, while it increased to around 30% when the enzyme was present. Lipases are known to accelerate the hydrolysis of the ester linkage. Moreover, in comparison with neat PBAT, the PBAT/TPS blend exhibited a higher susceptibility to biodegradation. This effect was expected and in agreement with literature data,[14,42] due to the higher sensitivity of starch to biological digestion. However, at the same TPS content, the blend containing LCNFs showed a lower degradation degree of about 17% after 10 days. This slight decrease may be due to the lower hydrophilicity of the film containing LCNFs, which reduces the diffusion of water inside the film.

Overall, the inclusion of LCNFs in PBAT/TPS-LCNF blends offers a sustainable, fully biobased alternative to improve the mechanical properties and mitigate water sensitivity in PBAT/TPS blends, without compromising the biodegradability of this class of commercial biodegradable

Table 2. Mechanical Data from Tensile Tests of the Blown Films

	ED			TD		
samples	US (MPa)	E (MPa)	σ_b (MPa)	US (MPa)	E (MPa)	σ_b (MPa)
PBAT	9.1	125	10.9			
PBAT/TPS 60/40	6.2	140	14.7	4.47	85	14.7
PBAT/TPS 60/40−8%LCNFs	7.9	171	16.2	5.33	125	9.1
PBAT/TPS 50/50	5.1	60	6.1	2.1	40	7.9
PBAT/TPS 50/50−8%LCNFs	5.9	63	12.6	3.40	70	7.8

https://doi.org/10.1021/acssuschemeng.4c02245
ACS Sustainable Chem. Eng. 2024, 12, 10805−10819

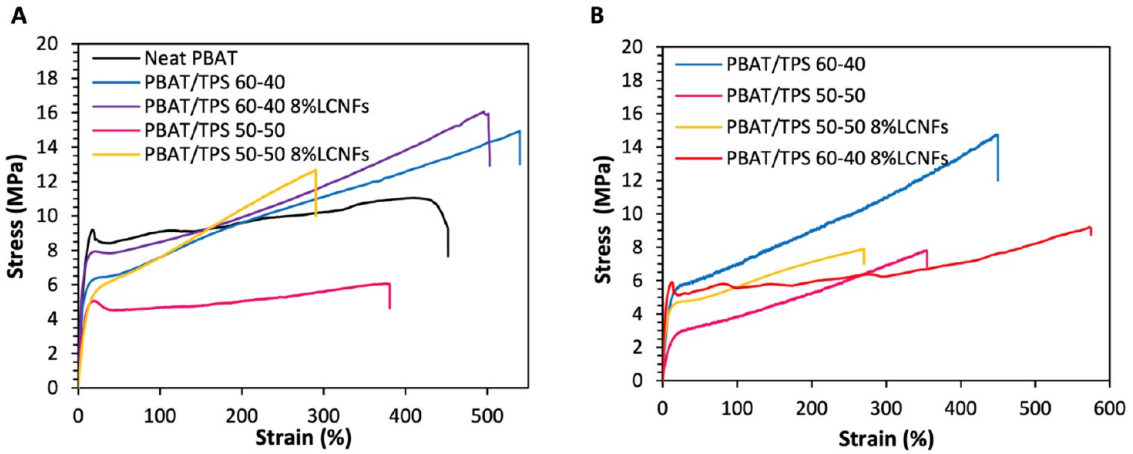

Figure 11. Tensile tests of the blown films in the (A) extrusion direction (ED) and (B) transverse direction (TD).

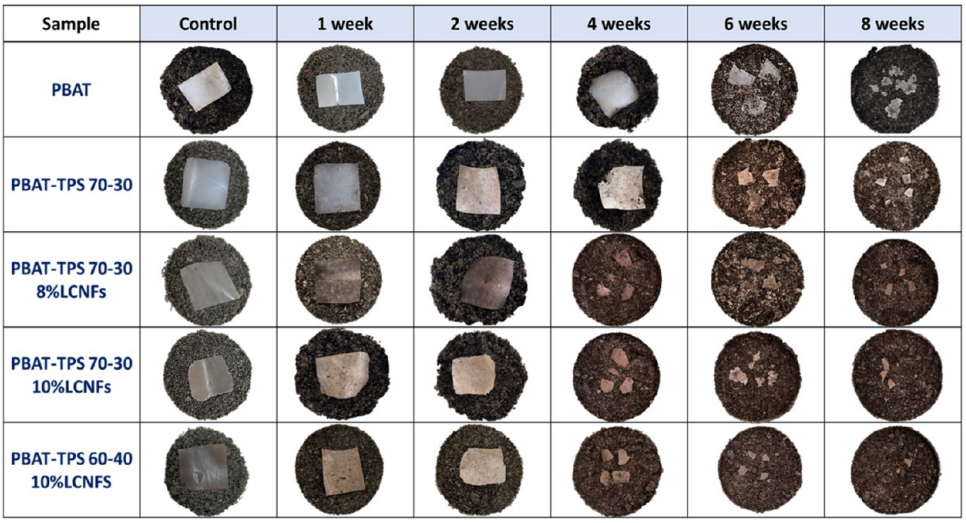

Figure 12. Evolution of the films after different burial times in soil at 58 °C.

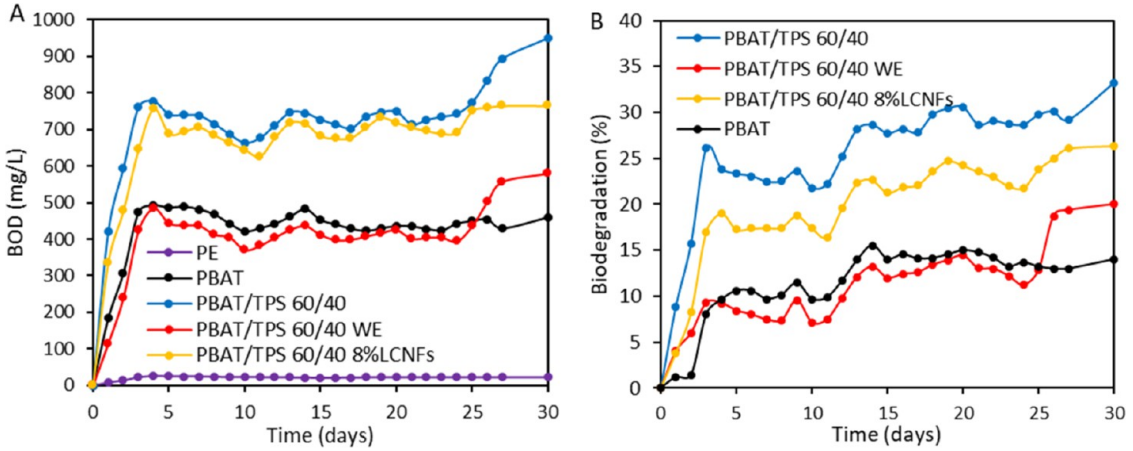

Figure 13. BOD measurement in an aqueous medium (A) and biodegradability of PBAT, PBAT/TPS 60/40 without enzymes (WE), PBAT/TPS 60/40, and PBAT/TPS 60/40−8%LCNFs (B).

plastic. Scheme 1 depicts the contribution of each component in the PBAT/TPS-LCNF blend to the properties of the film.

4. CONCLUSIONS

This study addresses a significant limitation in conventional PBAT/TPS blends, where the TPS content is typically capped at 20−30 wt % due to its detrimental effects on mechanical properties and increased water sensitivity. To overcome this

https://doi.org/10.1021/acssuschemeng.4c02245
ACS Sustainable Chem. Eng. 2024, 12, 10805−10819

Scheme 1. Illustrative Scheme of the Microstructure of PBAT/TPS-LCNF Blends with an Indication of the Contribution of Each Component to the Properties of the Film

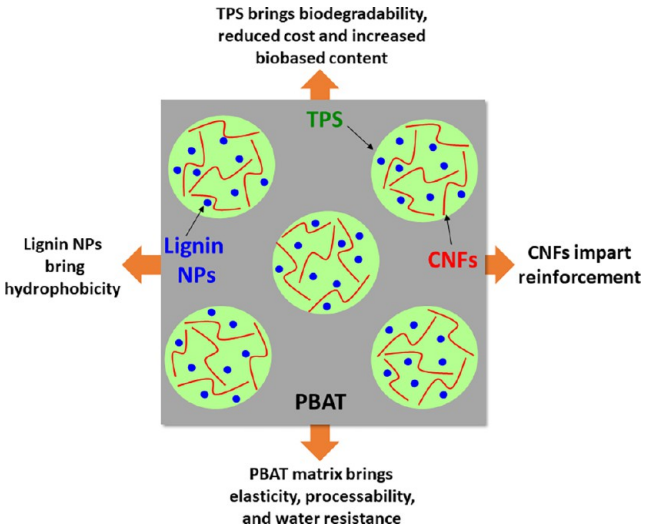

challenge, LCNFs were incorporated into PBAT/TPS blends, resulting in noteworthy improvements in water sensitivity and a substantial increase in the amount of low-cost TPS in PBAT/TPS blends. Moreover, the addition of LCNFs had a beneficial effect on the mechanical properties of the film, despite the increment in TPS content, without compromising ductility. Indeed, with 10 wt % LCNFs, films with 40 wt % TPS exhibited superior strength and stiffness compared to the neat PBAT matrix. SEM images revealed a nodular morphology of the TPS phase within the PBAT matrix up to a 50 wt % TPS content, with an increase in the size of the nodules with increasing LCNF content. The melt stiffness also increased with LCNF addition, influencing the morphology and contributing to improving mechanical properties. Interestingly, the addition of LCNFs resulted in a substantial reduction in moisture sorption, addressing the water sensitivity issue associated with PBAT/TPS blends. This reduction was attributed to the hydrophobic nature of lignin, which altered the hydrophilicity of the TPS phase. As a proof of concept to demonstrate that the inclusion of LCNFs did not impact the processability of the PBAT/TPS blends by extrusion-blowing, pilot tests were performed to produce thin films by blown-film extrusion with different TPS and LCNF contents. For all tested compositions, blown extrusion was successfully carried out without any instability or defects in the bubble. The mechanical testing of the films revealed improved properties, supporting the scalability of LCNF-incorporating PBAT/TPS blends for practical applications. The incorporation of LCNFs proved to be a promising strategy to overcome the limitations of conventional PBAT/TPS blends, offering a sustainable and biobased alternative with improved mechanical performance, reduced water sensitivity, and enhanced processability for various applications in the field of biodegradable polymers.

■ ASSOCIATED CONTENT

Supporting Information

The Supporting Information is available free of charge at https://pubs.acs.org/doi/10.1021/acssuschemeng.4c02245.

Processing route of PBAT/TPS-LCNF blends using a DSM-Xplore15cc Microextruder (Figure S1); photos showing the visual aspect of the PBAT/TPS-LCNF films incorporating different LCNF contents (Figure S2); complex viscosity $\eta*$ of PBAT and PBAT/TPS 70/30 % at different LCNF contents (A) and PBAT/TPS containing 10 wt % LCNFs at different PBAT/TPS ratios (B) (Figure S3); X-ray diffraction profile of an LCNF film. The peak indexes are those of allomorph I (Figure S4); SEM micrographs of cryogenically fractured surfaces for PBAT/TPS (70/30) at different LCNF contents: (A) 0 wt %, (B) 6 wt %, (C) 8 wt %, and (D) 10 wt %. The films were treated with 1 M HCl in order to etch away the TPS phase. The size distribution histograms of the resulting pores thus correspond to that of the TPS phase dispersed in the PBAT matrix. The pore size was measured for each blend using the ImageJ software: (E) 0 wt %, (F) 6 wt %, (G) 8 wt %, and (H) 10 wt % (Figure S5); SEM micrographs of cryofractured surfaces of PBAT/TPS-8% LCNF films with different PBAT/TPS ratios: (A) 70/30, (B) 60/40, and (C) 50/50. A treatment in 1 M HCl was performed to etch away the TPS phase (Figure S6); water contact angle of TPS and PBAT/TPS blends incorporating different LCNF contents (Figure S7); water sorption vs. time under immersion conditions for PBAT/TPS blends at different ratios and LCNF contents (Figure S8) (PDF)

■ AUTHOR INFORMATION

Corresponding Author

Sami Boufi − *University of Sfax, LMSE - Faculty of Science, 3018 Sfax, Tunisia;* orcid.org/0000-0002-3153-0288; Phone: 216 47274400; Email: sami.boufi@fss.rnu.tn; Fax: 216 74274437

Authors

Mohamed Aouay − *University of Sfax, LMSE - Faculty of Science, 3018 Sfax, Tunisia*

Albert Magnin − *Univ. Grenoble Alpes, CNRS, Grenoble INP, LRP, F-38000 Grenoble, France*

Christine Lancelon-Pin − *Univ. Grenoble Alpes, CNRS, CERMAV, F-38000 Grenoble, France*

Jean-Luc Putaux − *Univ. Grenoble Alpes, CNRS, CERMAV, F-38000 Grenoble, France;* orcid.org/0000-0002-9760-5369

Complete contact information is available at: https://pubs.acs.org/10.1021/acssuschemeng.4c02245

Notes

The authors declare no competing financial interest.

■ ACKNOWLEDGMENTS

The authors acknowledge LabEx Tec 21 (Investissements d'Avenir #ANR-11-LABX-0030) as well as the PHC Utique 23G1118 and Glyco@Alps programmes (Investissements d'Avenir #ANR-15-IDEX-02) for financial support. We thank the NanoBio-ICMG Platform (UAR 2607, Grenoble) for granting access to the Electron Microscopy facility. The Partenariat Hubert Curien (CMCU project: 23G1118) is gratefully acknowledged for its financial support. CERMAV and LRP are part of Institut Carnot PolyNat (Investissements

d'Avenir #ANR-11-CARN-030-01). The authors would like to thank the analytical chemistry platform of UFR Chemistry and Biology for providing facilities and Philippe Le Pellec for assistance.

REFERENCES

(1) Rojo, E.; Peresin, M. S.; Sampson, W. W.; Hoeger, I. C.; Vartiainen, J.; Laine, J.; Rojas, O. J. Comprehensive elucidation of the effect of residual lignin on the physical, barrier, mechanical and surface properties of nanocellulose films. *Green Chem.* **2015**, *17*, 1853−1866.
(2) Solala, I.; Iglesias, M. C.; Peresin, M. S. On the potential of lignin-containing cellulose nanofibrils (LCNFs): a review on properties and applications. *Cellulose* **2020**, *27*, 1853−1877.
(3) Al-Itry, R.; Lamnawar, K.; Maazouz, A. Biopolymer Blends Based on Poly (lactic acid): Shear and Elongation Rheology/Structure/Blowing Process Relationships. *Polymers* **2015**, *7*, 939−962.
(4) Sultana, A.; Kumar, L.; Gaikwad, K. K. Lignocellulose nanofibrils/guar gum-based ethylene scavenging composite film integrated with zeolitic imidazolate framework-8 for food packaging. *Int. J. Biol. Macromol.* **2023**, *243*, No. 125031.
(5) Zhang, X.; Tanguy, N. R.; Chen, H.; Zhao, Y.; Gnanasekar, P.; Le Lagadec, R.; Yan, N. Lignocellulosic nanofibrils as multifunctional component for high-performance packaging applications. *Mater. Today Commun.* **2022**, *31*, No. 103630.
(6) Fu, L.; Fang, Z.; Chen, H.; Wang, A.; Sun, C.; Zhai, Y.; Liu, W.; Qiao, Z.; Wen, Y. Fabrication of versatile lignocellulose nanofibril/polymerizable deep eutectic solvent hydrogels with anti-swelling, adhesive and low-temperature resistant properties via a one-pot strategy. *Int. J. Biol. Macromol.* **2024**, *256*, No. 128289.
(7) Wang, Y.; Liu, S.; Wang, Q.; Ji, X.; Yang, G.; Chen, J.; Fatehi, P. Strong, ductile and biodegradable polylactic acid/lignin-containing cellulose nanofibril composites with improved thermal and barrier properties. *Ind. Crops Prod.* **2021**, *171*, No. 113898.
(8) Zhang, C.-W.; Nair, S. S.; Chen, H.; Yan, N.; Farnood, R.; Li, F.-Y. Thermally stable, enhanced water barrier, high strength starch biocomposite reinforced with lignin containing cellulose nanofibrils. *Carbohydr. Polym.* **2020**, *230*, No. 115626.
(9) Ago, M.; Ferrer, A.; Rojas, O. J. Starch-Based Biofoams Reinforced with Lignocellulose Nanofibrils from Residual Palm Empty Fruit Bunches: Water Sorption and Mechanical Strength. *ACS Sustainable Chem. Eng.* **2016**, *4*, 5546−5552.
(10) Nair, S. S.; Chen, H.; Peng, Y.; Huang, Y.; Yan, N. Polylactic Acid Biocomposites Reinforced with Nanocellulose Fibrils with High Lignin Content for Improved Mechanical, Thermal, and Barrier Properties. *ACS Sustainable Chem. Eng.* **2018**, *6*, 10058−10068.
(11) Nair, S. S.; Yan, N. Effect of high residual lignin on the thermal stability of nanofibrils and its enhanced mechanical performance in aqueous environments. *Cellulose* **2015**, *22*, 3137−3150.
(12) Muller, J.; González-Martínez, C.; Chiralt, A. Combination of Poly(lactic) Acid and Starch for Biodegradable Food Packaging. *Materials* **2017**, *10*, 952.
(13) Ayu, R. S.; Khalina, A.; Harmaen, A. S.; Zaman, K.; Mohd Nurrazi, N.; Isma, T.; Lee, C. H. Effect of Empty Fruit Brunch reinforcement in PolyButylene-Succinate/Modified Tapioca Starch blend for Agricultural Mulch Films. *Sci. Rep.* **2020**, *10*, No. 1166.
(14) Dammak, M.; Fourati, Y.; Tarrés, Q.; Delgado-Aguilar, M.; Mutjé, P.; Boufi, S. Blends of PBAT with plasticized starch for packaging applications: Mechanical properties, rheological behaviour and biodegradability. *Ind. Crops Prod.* **2020**, *144*, No. 112061.
(15) Surendren, A.; Mohanty, A. K.; Liu, Q.; Misra, M. A review of biodegradable thermoplastic starches, their blends and composites: recent developments and opportunities for single-use plastic packaging alternatives. *Green Chem.* **2022**, *24*, 8606−8636.
(16) Nevoralová, M.; Koutný, M.; Ujčić, A.; Starý, Z.; Šerá, J.; Vlková, H.; Šlouf, M.; Fortelný, I.; Kruliš, Z. Structure Characterization and Biodegradation Rate of Poly(ε-caprolactone)/Starch Blends. *Front. Mater.* **2020**, *7*, No. 487523.
(17) Raquez, J. M.; Nabar, Y.; Narayan, R.; Dubois, P. In situ compatibilization of maleated thermoplastic starch/polyester melt-blends by reactive extrusion. *Polym. Eng. Sci.* **2008**, *48*, 1747−1754.
(18) Li, H.; Huneault, M. A. Effect of chain extension on the properties of PLA/TPS blends. *J. Appl. Polym. Sci.* **2011**, *122*, 134−141.
(19) Mallet, B.; Lamnawar, K.; Maazouz, A. Improvement of blown film extrusion of poly(Lactic Acid): Structure−Processing−Properties relationships. *Polym. Eng. Sci.* **2014**, *54*, 840−857.
(20) Sun, M.; Zhang, L.; Li, C. Modified cellulose nanocrystals based on SI-ATRP for enhancing interfacial compatibility and mechanical performance of biodegradable PLA/PBAT blend. *Polym. Compos.* **2022**, *43*, 3753−3764.
(21) da Costa, F. A. T.; Parra, D. F.; Cardoso, E. C. L.; Güven, O. PLA, PBAT, Cellulose Nanocrystals (CNCs), and Their Blends: Biodegradation, Compatibilization, and Nanoparticle Interactions. *J. Polym. Environ.* **2023**, *31*, 4662−4690.
(22) Alidadi-Shamsabadi, M.; Behzad, T.; Bagheri, R.; Nari-Nasrabadi, B. Preparation and characterization of low-density polyethylene/thermoplastic starch composites reinforced by cellulose nanofibers. *Polym. Compos.* **2015**, *36*, 2309−2316.
(23) Ahmadi, M.; Behzad, T.; Bagheri, R.; Heidarian, P. Effect of cellulose nanofibers and acetylated cellulose nanofibers on the properties of low-density polyethylene/thermoplastic starch blends. *Polym. Int.* **2018**, *67*, 993−1002.
(24) da Silva, J. B. A.; Santana, J. S.; de Almeida Lucas, A.; Passador, F. R.; de Sousa Costa, L. A.; Pereira, F. V.; Druzian, J. I. PBAT/TPS-nanowhiskers blends preparation and application as food packaging. *J. Appl. Polym. Sci.* **2019**, *136*, No. 47699.
(25) da Silva, J. B. A.; Bretas, R. E. S.; Lucas, A. A.; Marini, J.; da Silva, A. B.; Santana, J. S.; Pereira, F. V.; Druzian, J. I. Rheological, mechanical, thermal, and morphological properties of blends poly(butylene adipate-co-terephthalate), thermoplastic starch, and cellulose nanoparticles. *Polym. Eng. Sci.* **2020**, *60*, 1482−1493.
(26) Li, M.; Jia, Y.; Shen, X.; Shen, T.; Tan, Z.; Zhuang, W.; Zhao, G.; Zhu, C.; Ying, H. Investigation into lignin modified PBAT/thermoplastic starch composites: Thermal, mechanical, rheological and water absorption properties. *Ind. Crops Prod.* **2021**, *171*, No. 113916.
(27) Fourati, Y.; Tarrés, Q.; Delgado-Aguilar, M.; Mutjé, P.; Boufi, S. Cellulose nanofibrils reinforced PBAT/TPS blends: Mechanical and rheological properties. *Int. J. Biol. Macromol.* **2021**, *183*, 267−275.
(28) Najahi, A.; Tarrés, Q.; Delgado-Aguilar, M.; Putaux, J. L.; Boufi, S. High-Lignin-Containing Cellulose Nanofibrils from Date Palm Waste Produced by Hydrothermal Treatment in the Presence of Maleic Acid. *Biomacromolecules* **2023**, *24*, 3872−3886.
(29) Maréchal, Y.; Chanzy, H. The hydrogen bond network in Iβ cellulose as observed by infrared spectrometry. *J. Mol. Struct.* **2000**, *523*, 183−196.
(30) Faix, O. Investigation of Lignin Polymer Models (DHP's) by FTIR Spectroscopy. *Holzforschung* **1986**, *40*, 273−280.
(31) Tom, C.; Sangitra, S. N.; Pujala, R. K. Rheological fingerprinting and applications of cellulose nanocrystal based composites: A review. *J. Mol. Liq.* **2023**, *370*, No. 121011.
(32) Triacca, V. J.; Ziaee, S.; Barlow, J. W.; Keskkula, H.; Paul, D. R. Reactive compatibilization of blends of nylon 6 and ABS materials. *Polymer* **1991**, *32*, 1401−1413.
(33) Palierne, J. F. Linear rheology of viscoelastic emulsions with interfacial tension. *Rheol. Acta* **1990**, *29*, 204−214.
(34) Wadaugsorn, K.; Panrong, T.; Wongphan, P.; Harnkarnsujarit, N. Plasticized hydroxypropyl cassava starch blended PBAT for improved clarity blown films: Morphology and properties. *Ind. Crops Prod.* **2022**, *176*, No. 114311.
(35) Le, C. A. K.; Choisnard, L.; Wouessidjewe, D.; Putaux, J.-L. Polymorphism of crystalline complexes of amylose with fatty acids. *Int. J. Biol. Macromol.* **2018**, *119*, 555−564.
(36) van Soest, J. J. G.; Hulleman, S. H. D.; de Wit, D.; Vliegenthart, J. F. G. Crystallinity in starch bioplastics. *Ind. Crops Prod.* **1996**, *5*, 11−22.

https://doi.org/10.1021/acssuschemeng.4c02245
ACS Sustainable Chem. Eng. 2024, 12, 10805−10819

(37) Faker, M.; Razavi Aghjeh, M. K.; Ghaffari, M.; Seyyedi, S. A. Rheology, morphology and mechanical properties of polyethylene/ethylene vinyl acetate copolymer (PE/EVA) blends. *Eur. Polym. J.* **2008**, *44*, 1834−1842.
(38) Fourati, Y.; Tarrés, Q.; Mutjé, P.; Boufi, S. PBAT/thermoplastic starch blends: effect of compatibilizers on the rheological, mechanical and morphological properties. *Carbohydr. Polym.* **2018**, *199*, 1−57.
(39) Moustafa, H.; Guizani, C.; Dupont, C.; Martin, V.; Jeguirim, M.; Dufresne, A. Utilization of torrefied coffee grounds as reinforcing agent to produce high-quality biodegradable PBAT composites for food packaging applications. *ACS Sustainable Chem. Eng.* **2017**, *5* (2), 1906−1916.
(40) Forssell, P. M.; Mikkilä, J. M.; Moates, G. K.; Parker, R. Phase and glass transition behaviour of concentrated barley starch-glycerol-water mixtures, a model for thermoplastic starch. *Carbohydr. Polym.* **1997**, *34*, 275−282.
(41) Ter Halle, A.; Ladirat, L.; Gendre, X.; Goudouneche, D.; Pusineri, C.; Routaboul, C.; Tenailleau, C.; Duployer, B.; Perez, E. Understanding the Fragmentation Pattern of Marine Plastic Debris. *Environ. Sci. Technol.* **2016**, *50*, 5668−5675.
(42) Mohanty, S.; Nayak, S. K. Starch based biodegradable PBAT nanocomposites: Effect of starch modification on mechanical, thermal, morphological and biodegradability behavior. *Int. J. Plast. Technol.* **2009**, *13*, 163−185.

https://doi.org/10.1021/acssuschemeng.4c02245
ACS Sustainable Chem. Eng. 2024, 12, 10805−10819